

Ions Tune Interfacial Water Structure and Modulate Hydrophobic Interactions at Silica Surfaces

Aashish Tuladhar,^{||} Shalaka Dewan,^{||} Simone Pezzotti,^{||} Flavio Siro Brigiano, Fabrizio Creazzo, Marie-Pierre Gaigeot,^{*} and Eric Borguet^{*}

Cite This: *J. Am. Chem. Soc.* 2020, 142, 6991–7000

Read Online

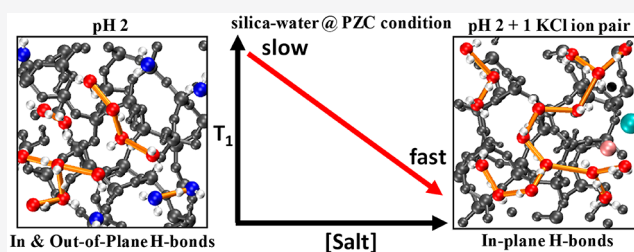
ACCESS |

Metrics & More

Article Recommendations

Supporting Information

ABSTRACT: The structure and ultrafast dynamics of the electric double layer (EDL) are central to chemical reactivity and physical properties at solid/aqueous interfaces. While the Gouy–Chapman–Stern model is widely used to describe EDLs, it is solely based on the macroscopic electrostatic attraction of electrolytes for the charged surfaces. Structure and dynamics in the Stern layer are, however, more complex because of competing effects due to the localized surface charge distribution, surface–solvent–ion correlations, and the interfacial hydrogen bonding environment. Here, we report combined time-resolved vibrational sum frequency generation (TR-vSFG) spectroscopy with *ab initio* DFT-based molecular dynamics simulations (AIMD/DFT-MD) to get direct access to the molecular-level understanding of how ions change the structure and dynamics of the EDL. We show that innersphere adsorbed ions tune the hydrophobicity of the silica–aqueous interface by shifting the structural makeup in the Stern layer from dominant water–surface interactions to water–water interactions. This drives an initially inhomogeneous interfacial water coordination landscape observed at the neat interface toward a homogeneous, highly interconnected in-plane 2D hydrogen bonding (2D-HB) network at the ionic interface, reminiscent of the canonical, hydrophobic air–water interface. This ion-induced transformation results in a characteristic decrease of the vibrational lifetime (T_1) of excited interfacial O–H stretching modes from $T_1 \sim 600$ fs to $T_1 \sim 250$ fs. Hence, we propose that the T_1 determined by TR-vSFG in combination with DFT-MD simulations can be widely used for a quantitative spectroscopic probe of the ion kosmotropic/chaotropic effect at aqueous interfaces as well as of the ion-induced surface hydrophobicity.



INTRODUCTION

Water is critical to sustaining life on Earth, and knowledge about its chemistry and physics is central to a vast range of subjects.^{1–11} However, the organization of water in inhomogeneous environments remains controversial, owing to water's many anomalous properties.¹² A simple question such as how far away ions can affect the physical and the chemical properties of water is still rigorously debated.^{13–20} To make matters worse, understanding the behavior of water and solvated ions at an interface is an even more arduous task. Intuitively, it is fairly obvious that when ions approach an interface, they screen the surface charge (if present) and also (most likely) reorganize the interfacial environment by restructuring the original surface–solvent and solvent–solvent interactions since competing ion–solvent, ion–surface, and ion–ion interactions are introduced. Therefore, a quantitative and molecular-level understanding of these interactions is essential to understand and predict ion activity at interfaces and their influence on chemical reactivity.

The mineral oxide–electrolyte aqueous interface provides an excellent platform to investigate surface–ion–solvent interactions as a function of surface charge by manipulating the pH

of the bulk aqueous solution across the point of zero charge (PZC) of the mineral, hence tuning the electrostatic attraction between the surface and the ions. The silica–water interface represents the most widely studied mineral–aqueous interface. Therefore, many spectroscopic and imaging techniques have been used extensively to study the electric double layer (EDL) at the silica–electrolyte interface.^{21–26} The EDL can be broadly subdivided into a Stern layer located within the first one/two aqueous monolayers from the solid surface where ions accumulate, followed by a diffuse layer consisting of solvated ions that screen the remaining surface charge.^{27,28} While the energetics of the diffuse layer is reasonably well approximated by the Gouy–Chapman (GC) model, the understanding of the Stern layer is still limited. This is largely because the structure and dynamics of the Stern layer are

Received: December 10, 2019

Published: April 1, 2020



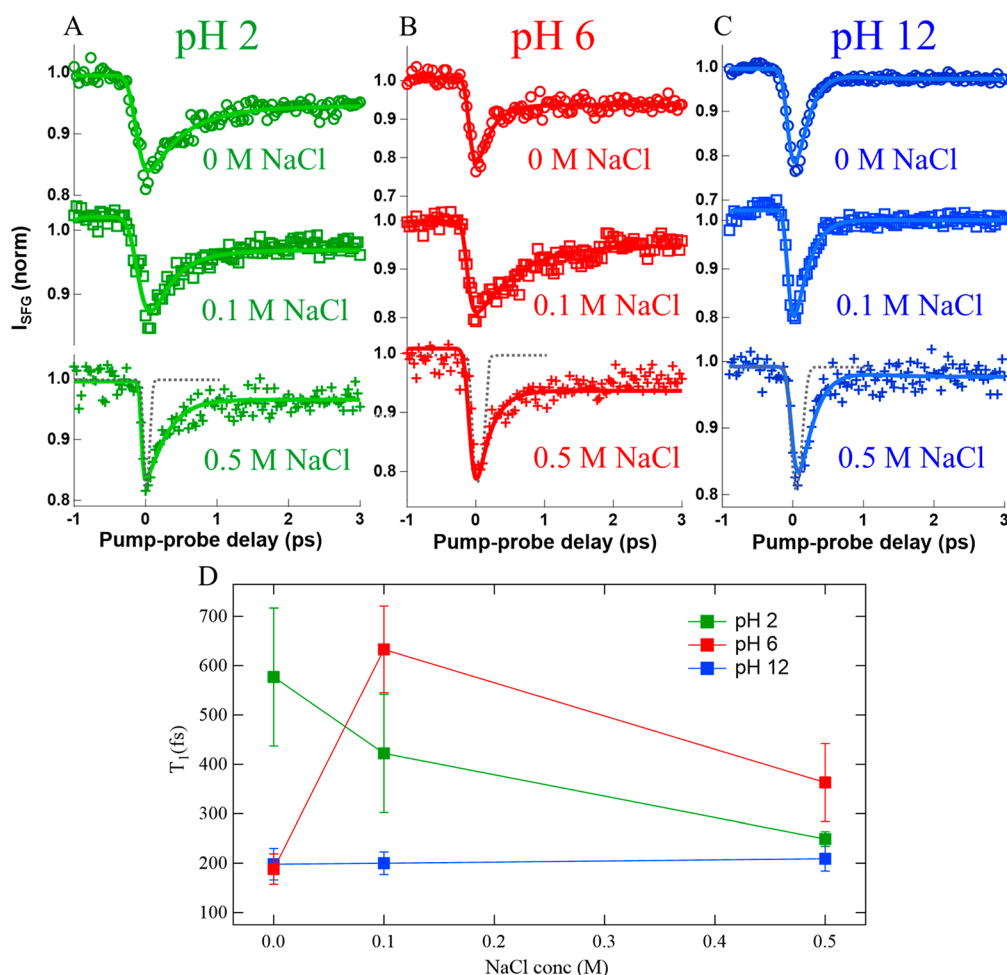


Figure 1. Effect of ions on the vibrational dynamics of the O–H stretch in H₂O at the silica–water interface at (A) pH 2, (B) pH 6, and (C) pH 12. The gray dotted line represents the cross-correlation of the IR pump, IR probe, and visible pulses, i.e., the instrument response function, indicating a fwhm of ~ 120 fs. The solid lines are the best fits with a four-level system, described in the Supporting Information. (D) T_1 (O–H vibrational lifetime) vs NaCl concentration. The T_1 values reported are the average T_1 from separate measurements repeated at least 3 times, and in some cases up to 5 times. The error bars indicate the standard deviation for all the individual T_1 values obtained on different days.

directly sensitive to the competing effects of the surface charge distribution, surface–solvent–ion correlations, and the interfacial hydrogen bonding environment, which are all extremely difficult to probe experimentally. Hence, the detailed understanding of these interfacial properties is not accounted for in the most commonly used Stern–Gouy–Chapman (SGC) model. Therefore, experimental tools that can provide quantitative and molecular understanding of the EDL are key to the development of more sophisticated models that can accurately describe its structure, composition, and energetics.

Vibrational sum frequency generation (vSFG) spectroscopy, a laser-based second-order nonlinear optical technique, has played a key role in the last few decades in advancing our understanding of the EDL structure at the silica–electrolyte interface.^{21,22,24,29–33} In a typical vSFG experiment, an infrared (IR) laser beam which is in resonance with a molecular vibration is temporally and spatially overlapped with a visible laser at an interface of interest, resulting in the generation of sum frequency (SF) photons whose frequency is the sum of the IR and visible frequencies. Within the dipole approximation, only noncentrosymmetric molecules and environments generate a vSFG signal. Centrosymmetry is inherently broken at any interface between two bulk media, thus making vSFG spectroscopy an exclusive probe of molecular vibrations

at the interface and hence an ideal tool for probing the EDL. Moreover, vSFG can be employed in both the frequency domain (steady-state (SS) vSFG) and the time-domain (time-resolved (TR) vSFG) to extract structural and dynamics information on the EDL. Despite a plethora of investigations of the silica–electrolyte interface using SS-vSFG^{31,34–40} and TR-vSFG,^{21,22,41,42} a complete molecular picture of the silica–electrolyte EDL is still lacking. This mainly stems from two critical shortcomings in past vSFG studies.

The first issue is due to the ambiguity of the probing depth of vSFG at charged interfaces (the silica–water interface is habitually charged except at its PZC, around pH 2–4) where the surface electric field can break the centrosymmetry of bulklike water residing further than the first few interfacial layers and hence contributing to, or even dominating, the vSFG signal. This has greatly complicated the interpretation of vSFG studies of silica–water interfaces and has impeded a definitive rationalization of the structure and dynamics of the EDL, since it is unclear which populations (interfacial water or electric field-oriented bulklike water) are probed. However, recent experimental⁴³ and computational⁴⁴ studies have developed methodologies to separate vSFG spectra into contributions originating from the first few layers [binding interfacial layer (BIL)] and from the electric field oriented

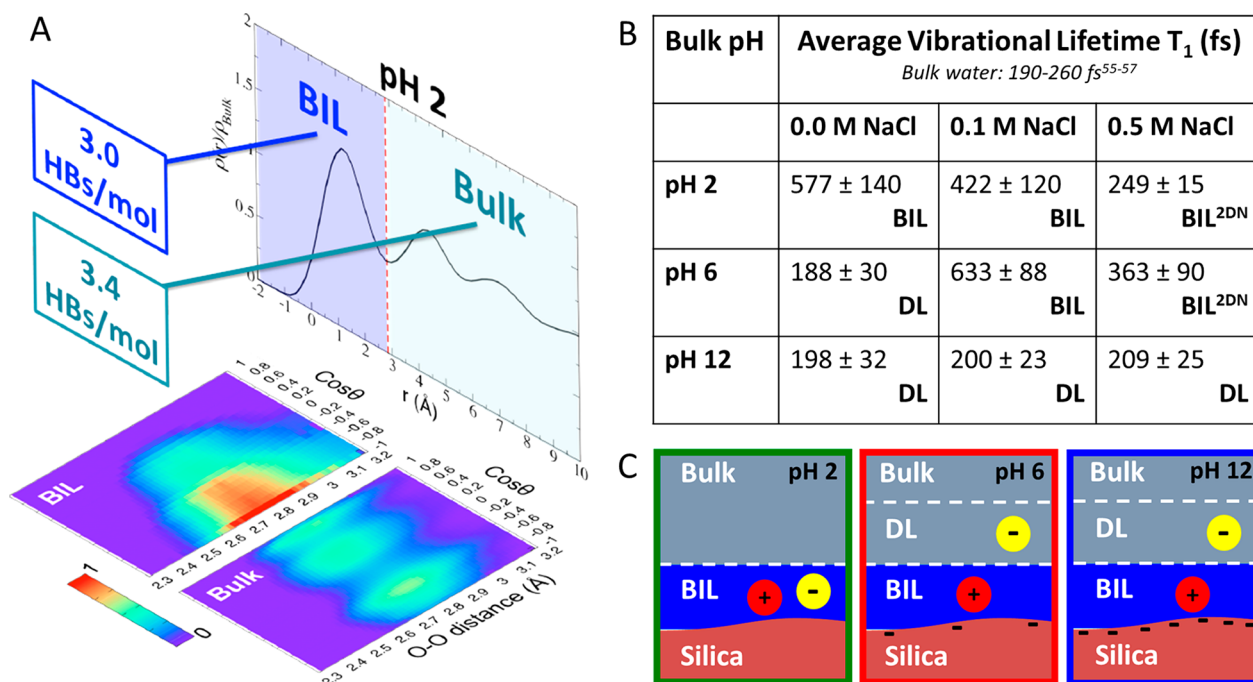


Figure 2. (A) Three descriptors used for characterizing and determining water BIL/DL/Bulk layers at the neat silica–water interface at pH 2. They are (see refs 44, 54, and 55) the water density profile with respect to the distance from the surface (r), the average water coordination (HBs/molecule), and the 3D-plots evaluating the probability for water–water HBs formed in each layer with a given HB (O–O) distance and orientation with respect to the normal to the surface (red regions correspond to the maximum probability to find water with preferential HB distances and orientations; see Section S6 in the SI for details). See all details in Section S5 of the SI. (B) Average vibrational lifetime T_1 at different bulk pH and NaCl concentrations, obtained from 4 level model fits (described in the SI) to TR-vSFG traces. The error bars indicate the standard deviation for all the individual T_1 values obtained on different days. The labels “BIL” (binding interfacial layer), “BIL^{2DN}” (2DN stands for the 2D–H bond-network formed by the BIL water), and “DL” (diffuse layer) refer to the interfacial region that dominates the vSFG response in each aqueous environment, as described in the text. (C) Schemes of the structural organization of water and ions at the 1 M electrolytic amorphous silica–water interface (pH = 2, 6, 12) extracted from the AIMD/DFT-MD simulations. Red/yellow balls with +/– signs represent the cations/anions and their distribution at the interface (BIL vs DL).

bulklike contribution [diffuse layer (DL)]. The BIL water region is analogous to the Stern layer in the double layer theory from the aspect of the spatial distribution of the ions.⁴³ Only recently, this methodology has been applied to vSFG studies of the fused silica–aqueous interface revealing important insight on its chemical and physical properties (for example, microscopic hydrophobicity).^{29,74}

The second shortcoming stems from the lack of understanding of how the presence of ions affects the vSFG signal. Historically, the ion associated attenuation of the vSFG signal at the silica–aqueous interface has been assigned to the Debye screening effect (as predicted by GC theory); i.e., ions reduce the thickness of the non-centrosymmetric diffuse layer probed by vSFG. It is also obvious that ions can rearrange the interfacial hydrogen-bonding environment due to ion–solvent and ion–surface interactions. However, it is unclear how ion-induced screening and ion-induced solvent rearrangement affect the vSFG signal. The need to look beyond the GC/SGC models to understand the silica–electrolyte EDL, in order to disclose the more complex molecular-level rearrangements occurring in the BIL, is the missing ingredient for the development of next-generation models describing ion activity at interfaces. The need for such development was, for instance, recently pointed out in nonlinear spectroscopy studies by Borguet et al.,³⁵ Gibbs et al.,²⁵ and Geiger et al.²³ where they provided evidence for highly pH-dependent specific ion effects, whose understanding is beyond the GC/SGC models. Here, we report a joint effort, combining time-resolved vibrational

sum frequency generation (TR-vSFG) spectroscopy with ab initio DFT-based molecular dynamics simulations (AIMD/DFT-MD), to reveal novel molecular details on how ions change the interfacial water structure in the BIL and consequently affect its ultrafast vibrational dynamics. TR-vSFG spectroscopy, measuring the vibrational relaxation time-scale of the O–H stretching vibrations, provides an excellent quantifiable probe of the hydrogen bonding environments of the silica–electrolyte EDL, allowing us to experimentally detect ion-induced changes in the BIL, which may otherwise be too subtle or nonexistent in the SS-vSFG signal.^{24,35} Complementarily, DFT-MD simulations provide a detailed understanding of the microscopic mechanism(s) resulting in the ion-induced effects on the TR-vSFG measurements. Our results clearly show that the GC/SGC models are insufficient in describing the ion activity at silica surfaces, and the molecular insights provided by this study could be significant in the development of more accurate and sophisticated EDL models that would account for the interface specific chemistry, surface charge and ion distribution, and the resulting hydrogen bonding environment.

RESULTS AND DISCUSSION

Time-Resolved Sum Frequency Generation. The vibrational dynamics of the silica–water interface, measured using TR-vSFG spectroscopy (experimental and sample preparation details are provided in the SI), is clearly a function of both bulk pH and ionic strength (Figures 1 and 2B). More

precisely, the water OH stretch T_1 lifetime is found to strongly depend on the ion concentration at pH 2 and 6, while a constant T_1 of ~ 200 fs is observed for pH 12 in the 0–0.5 M NaCl range. At pH ~ 12 , the silica surface is dehydroxylated by $\sim 25\%$,⁴⁵ inducing a rather high surface charge density of ~ -0.2 C/m², thus resulting in a surface potential of ~ 170 mV, as calculated using the silica deprotonation ratio and the GC model (described in Section S3 of the SI, see also Figures S4 and S5). There is therefore a strong water DL impact to vSFG due to the surface field-oriented bulklike water (see, e.g., refs 21, 22, 44, 46, and 47). Both the BIL and the DL impact the vSFG response, and their relative weighted contributions to the final TR-vSFG measurements can be qualitatively estimated from the surface potential by using the framework described hereafter. See Section S5 in the SI for the BIL/DL definition. The vSFG signal in the DL is due to the potential drop across the DL ($\Delta\varphi_{\text{DL}}$, assumed here as equal to the surface potential; see Table S2 for a comparison with other choices) through $\chi^{(2)}_{\text{DL}}(\omega) = \chi^{(3)}_{\text{bulk}}(\omega) \Delta\varphi_{\text{DL}}$,^{43,44,46} where $\chi^{(3)}_{\text{bulk}}(\omega)$ is the third-order susceptibility of bulk liquid water (this expression is here written without interference contributions^{48,49} which are only important at low ionic strength and hence trivial at pH 12 which has an ionic strength of 10 mM). $\chi^{(3)}_{\text{bulk}}(\omega)$ is known.^{43,44} In the present experiments, $|\chi^{(2)}(\omega)|^2$ signals are measured to deduce T_1 relaxation times; thus, $|\chi^{(2)}_{\text{DL}}(\omega)|^2 = |\chi^{(3)}_{\text{bulk}}(\omega)|^2 (\Delta\varphi_{\text{DL}})^2$. Defining I_{BIL} and I_{DL} as the integral of $\chi^{(2)}_{\text{BIL}}(\omega)$ and $\chi^{(2)}_{\text{DL}}(\omega)$ in the O–H stretching region, one finds that $I_{\text{DL}}/I_{\text{BIL}} \propto (\Delta\varphi_{\text{DL}})^2$, i.e., the ratio of DL/BIL intensities, is proportional to the square of the surface potential. According to previous works on silica–water interfaces,^{44,46} values of $I_{\text{DL}}/I_{\text{BIL}} \sim 10$ were found for $\Delta\varphi_{\text{DL}} \sim 10$ mV. Taking $\Delta\varphi_{\text{DL}} \sim 10$ mV as the reference ($(\Delta\varphi_{\text{DL}}(\text{ref}))$), we can estimate the $I_{\text{DL}}/I_{\text{BIL}}$ ratio at any other $\Delta\varphi_{\text{DL}}$ value as $I_{\text{DL}}/I_{\text{BIL}}(\Delta\varphi_{\text{DL}}) = I_{\text{DL}}/I_{\text{BIL}}(\Delta\varphi_{\text{DL}}(\text{ref})) \times (\Delta\varphi_{\text{DL}}/(\Delta\varphi_{\text{DL}}(\text{ref})))^2 = 10(\Delta\varphi_{\text{DL}}/10 \text{ mV})^2$. See Sections S9 and S10 for more details. Therefore, $I_{\text{DL}}/I_{\text{BIL}} \sim 2960$ is expected here for $\Delta\varphi_{\text{DL}} \sim 172$ mV at pH ~ 12 (see Table S2). The vSFG response at the neat pH ~ 12 silica–water interface is consequently dominated by the water in the DL, i.e., by bulklike oriented liquid, and indeed one measures $T_1 = 198 \pm 32$ fs (Figures 1 and 2B), typical of the 190–260 fs^{50–52} relaxation measured in bulk liquid water. When adding 0.1 and 0.5 M salt, the surface potential is reduced but is still of the order ~ 100 mV (see Table S2), thus giving rise to the same DL-dominated fast interfacial relaxation. These results suggest that higher concentrations than 0.5 M are needed to screen the silica surface potential and hence suppress the DL contribution to vSFG at pH ~ 12 . This is indeed the conclusion of the recent vSFG measurements by Tahara's group,⁴⁰ where 2 M NaCl is needed to measure only the BIL contribution at pH 12.

When lowering the pH to 6, the silica surface is now only $\sim 1\%$ dehydroxylated.⁴⁵ A smaller surface potential (~ 80 mV) is hence created, and in the absence of additional ions, $\Delta\varphi_{\text{DL}} \sim 80$ mV (Figure S5 in the SI). Correcting for interference effects, which now need to be considered for the neat pH 6 condition (where the ionic strength is 10^{-6}), an $I_{\text{DL}}/I_{\text{BIL}}$ ratio of 26 is obtained (see Sections S9 and S10 and Table S2 in the SI), still large enough to conclude that the measured relaxation time is dominated by the DL contribution. Consistently, we measure $T_1 = 188 \pm 30$ fs (Figures 1 and 2B), similar to pH 12 conditions. A recent study from Hore-Tyrodé³² reported a surface potential of ~ 200 mV for the same neat pH 6

conditions (i.e., no excess salt). Taking this larger surface potential value leads to an even larger $I_{\text{DL}}/I_{\text{BIL}}$ ratio, making our conclusion on dominant DL contributions even stronger.

Adding 0.1 or 0.5 M salt at pH ~ 6 results in an accumulation of cations at the negatively charged surface, hence reducing the surface potential by more than 1 order of magnitude (Figure S5 and Table S2, SI). We note here that addition of ions is known to increase the percentage of deprotonated sites.^{32,45,53} Despite the increase in deprotonation, the surface potential is lower than in the case of no salt (Figure S5B), as shown in a recent study.³² This is possibly due to the counterion screening the surface potential by directly interacting with the deprotonated SiO^- sites, as shown by a previous study.⁵³ Moreover, the surface potential is observed to decay exponentially away from the surface when salt is present (Figure S5) so that it is only 4 and 1 mV at 1 nm away from surface for 0.1 and 0.5 M NaCl, respectively. Due to the lower surface potential and rapid decay (see Figure S5 and Table S2 in the SI), the DL contribution to the vSFG signal is largely suppressed at pH 6 when salt is added.

In agreement with these estimates, we find that the presence of 0.1 M NaCl initially slows down T_1 to 633 fs, which is similar to the T_1 at neat pH 2. This means that the 0.1 M NaCl at pH 6 is mainly only responsible for screening surface charge, hence excluding the DL water contribution to T_1 lifetime, as one would expect from the GC model and consistent with a previous study.²² However, when the salt concentration is further increased to 0.5 M, T_1 becomes faster (363 fs), deviating from the behavior expected from GC theory. Since the surface potential is very low at pH 6 with 0.5 M [NaCl], the T_1 decrease has to arise from ion-induced changes in the BIL.

In analogy with the findings at pH 6, a similar BIL-specific effect is also observed for pH 2, point of zero charge (PZC) conditions, where the measured T_1 lifetimes (Figures 1 and 2B) show that the vibrational relaxation of water is accelerated by increasing the bulk ionic concentration. In the absence of salt, the surface potential is close to zero (Figure S5A and Table S2, SI) and we can consequently assume that the silica surface is neutral and that the vSFG probing depth and the T_1 lifetimes reflect the water structure in the BIL alone. When ions are introduced, the T_1 lifetime decreases from 577 fs for the neat interface to 422 fs for 0.1 M [NaCl] and to 249 fs for 0.5 M [NaCl], while the surface potential remains close to zero (Figure S5 and Table S2, SI). The BIL is thus expected to be solely responsible for the measured T_1 lifetime in the entire investigated concentration range at pH = 2, meaning that there is no preferential adsorption of cations over anions or vice versa, and both ionic species have the same probability to populate the BIL layer.

Here, it is important to consider the possibility of cations preferentially accumulating at the neutral silica surface compared to anions (as is known to occur at higher pH values, above PZC), resulting in a slightly positive surface so that the vSFG probes DL (“bulklike”) water via the $\chi^{(3)}$ effect and causing an acceleration of the T_1 . However, this scenario would manifest in a large DL-water contribution to the total SS-vSFG spectra. This was indeed reported in a recent vSFG study²⁴ which showed a significant increase in the vSFG signal at pH 2 when the NaCl concentration was raised from 10 to 100 mM, which was interpreted as an overcharging effect. However, the overcharging effect was mostly apparent for the ssp-vSFG signal and not for the ppp-vSFG signal. We use the

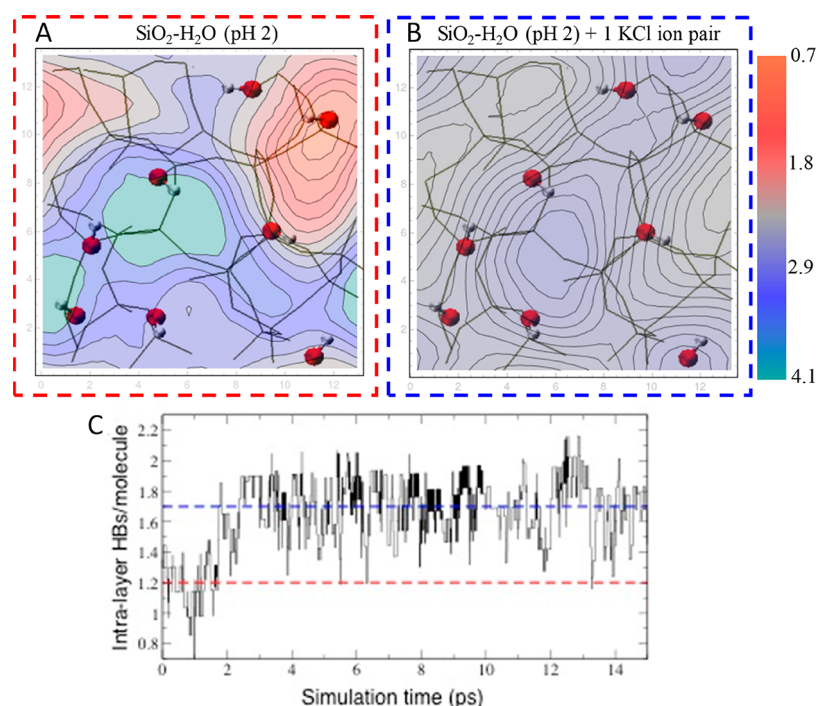


Figure 3. AIMD/DFT-MD simulations of the amorphous silica–water interface at pH \sim 2. Time-averaged coordination number of the water molecules in the BIL spatially resolved along the lateral x – y directions of the silica surface (in Å) for (A) neat aqueous silica interface and (B) aqueous silica interface with one KCl ion pair in the BIL. The water coordination is expressed in terms of the number of HBs (sum of water–water and water–silanol HBs) per water molecule (see Section S6 in the SI for details). The color coding (vertical scale in the plots) goes from light red (0.7 HBs/molecule), dark red (1.8 HBs/molecule), grayish-blue (2.9 HBs/molecule) to greenish-blue (4.1 HBs/molecule). The top view of the interface shows the solid Si–O covalent bonds in gray lines to highlight the solid surface covalent patterns. The surface silanols are marked by the O–H groups in red (O) and white (H) spheres. (C) Time-evolution of the number of intra-BIL HBs formed per water molecule located within the BIL. $t = 0$ is the time when a KCl ion-pair is introduced in the BIL. The red and blue dashed lines indicate the average number of intra-BIL HBs per water molecule for the neat interface (red, 1.2) and for the KCl electrolyte interface (blue, 1.7), respectively.

latter polarization combination in this study. Also, hysteresis has been reported when pH is varied at constant ionic strength, which is how the above-mentioned study was conducted. In our study, we vary the ionic strength at constant pH which avoids the hysteresis issue. We see no significant increase in SS-vSFG signal at pH 2 when NaCl concentration is increased (Figure S6), which is consistent with other past studies of silica–water interfaces at pH \sim 2 conditions³⁵ as well as with the estimated surface potential values (Figure S5A). On the contrary, we notice a small decrease in ppp-vSFG intensity with salt addition, which could also be in principle attributed to the screening effect of the electrolyte (by hypothesizing that a small net surface charge persists at pH 2). However, we also see an acceleration of T_1 when 0.1 M salt is added. Thus, the decrease in ppp-vSFG intensity cannot be entirely due to the screening effect. As we will show later, such a decrease can be explained when the ion-induced changes in the BIL water structure are considered.

In the light of all the above-discussed evidence, the accelerations of T_1 lifetimes at pH \sim 2 conditions and pH 6 with $[\text{NaCl}] = 0.1$ – 0.5 M are ascribed to ion inducing order and more interconnectivity within the structure of the BIL water, i.e., a kosmotropic effect. A deep understanding of the associated microscopic mechanism, which goes beyond pure electrostatic effects and is almost entirely driven by specific ion-induced changes in water–water and water–surface interactions, is pivotal in order to improve our comprehension and modeling of electrolytic interfaces. We hence now make use of DFT-MD simulations to address this challenge.

DFT Molecular Dynamics. A DFT-MD simulation of the aqueous amorphous silica surface ($4.5 \text{ SiOH}/\text{nm}^2$, representative of the silica surfaces in experiments) at pH 2 was performed (see Section S5 in the SI for all computational details). In agreement with the experimental results, the simulation shows that when the surface is neutral (pH \sim 2), only the water in the BIL is noncentrosymmetric and hence vSFG-active. This is summarized in Figure 2A, where water in the BIL is shown to be denser than in the bulk, forming fewer water–water HBs, and with a noncentrosymmetric orientation, while bulklike water coordination, orientation, and density are recovered right beyond the BIL, i.e., further than 3.0 \AA from the SiO_2 surface (see also Section S6 of the SI). The absence of a DL confirms that the aqueous silica interface is at the isoelectric point at pH \sim 2.

What the DFT-MD simulation also reveals is that the inhomogeneous spatial distribution of silanols at the amorphous silica surface results in a nonuniform spatial distribution of the coordination number of the water molecules in the BIL (Figure 3A, where the time averaged spatial distribution of the coordination number of water in the BIL is shown in a contour-map). Water coordination results from the sum of water–water and water–silanol HBs, where a standard HB definition is applied (O–O distance $< 3.2 \text{ \AA}$ and O(–H)–O angle in 140 – 220° interval).⁵⁴ If, on average, water is 3-fold coordinated in the BIL, this number is in fact due to two distinct populations: 60% of the water molecules in the BIL are tetrahedrally coordinated (HB/mol ≥ 3.1 , blue zones in Figure 3A), while the other 40% are undercoordinated (HB/mol < 2.2 ,

red zones). These two water populations are located above silica areas made of high (bottom half of Figure 3A and B) and low (top half of Figure 3A and B) silanol densities, respectively, which we have recently identified as hydrophilic/hydrophobic patches on the macroscopically hydrophilic silica surface.^{29,56}

To reveal how ions affect the BIL water structure and dynamics, eight additional DFT-MD simulations have been performed in the presence of a KCl ion-pair. In AIMD simulations, the Na⁺ cation is known to require much larger plane wave basis sets for its accurate electronic representation than K⁺, hence considerably increasing the computational cost of the AIMD, and, thus, the choice of K⁺ in the present simulations. The results obtained with KCl have been then confirmed with one supplementary MD simulation where one NaCl ion-pair is accommodated at the silica–water interface (see Section S8 in the SI). The similarity between Na⁺/K⁺ behaviors found in the present work is consistent with a previous study.⁵⁷ As already discussed, since the silica surface is at the isoelectric point at pH \sim 2, and no static field is generated by the neutral surface, there is no surface electrostatic driving force to favor cations over anions (and vice versa) to approach closer to the silica surface. Starting from this knowledge, nine distinct initial ion configurations have been prepared for the MD simulations, where both K⁺/Na⁺ and Cl⁻ ions were randomly located within the BIL layer (see Sections S4 and S8 of the SI).

We make the choice to discuss hereafter the results from one representative DFT-MD simulation, the results of which have been validated by all the other simulations (the total of nine simulations amounts to 150 ps time-scale), revealing that our findings are independent of the average position and configuration (i.e., contact ion-pair CIP, solvent shared ion-pairSSIP) that ions have in the BIL, as well as on the K⁺/Na⁺ nature of the cation (all detailed in Section S8 of the SI).

The resulting picture obtained from the DFT-MD simulations is the following. The presence of the electrolyte in the BIL leads to the BIL water becoming homogeneously 3-fold coordinated (Figure 3B); i.e., there is one single water population (91% of the water in the BIL), highly interconnected by H-bonds within the layer (1.7 intra-BIL HBs on average). This striking change in the water structural organization in the BIL from the neat to the electrolytic SiO₂–water interface is due to two combined factors: by approaching the silica surface, the ions are able to complete their solvation shell with surface silanols on top of BIL water molecules (i.e., ions adsorbed in innerspheres, see Figure 4C), as already shown at the crystalline quartz–water⁵⁸ and alumina–water⁵⁹ interfaces, thereby breaking local water–surface H-bonds that were previously present at the neat aqueous silica interface. Innersphere ions hence locally drive the breaking of water–surface interactions which is characteristic of the hydrophobic patches at the silica surface.^{29,56} They consequently increase the portion of the surface assigned to the hydrophobic domain. Above these ion-induced hydrophobic domains, water adapts to this change by maximizing H-bonds in between interfacial water molecules (intra-BIL HBs), hence increasing the water–water H-bond connectivity within the BIL. As a result of such an ion-catalyzed shift in the balance between water–water and water–surface interactions toward the former, a highly ordered water–water HB-network with HBs parallel to the silica surface plane is formed in the whole BIL, reminiscent of the 2D-HB-network recently revealed at

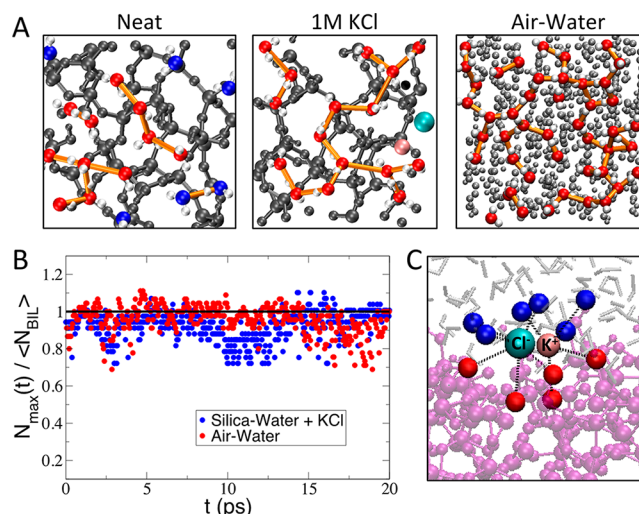


Figure 4. (A) Top views of the BIL water structural arrangement at the neat silica–water (left), the silica–water interface with one KCl ion pair in the BIL (middle), and the canonical hydrophobic air–water interface (right) used here as a reference for the highly interconnected H-bond network (2D-HB-network) formed by the water in the BIL.^{54,55} The silica surface atoms are black balls (left and middle), while the gray balls in the right-hand figure are the water in the bulk liquid. The water molecules in the BIL are color-coded according to their coordination number, i.e., blue if ≤ 2.2 HBs/mol, red if > 2.2 HBs/mol. In the absence of ions, water molecules with lower coordination number (blue) and with higher coordination number (red) are present, connected only by few H-bonds (orange). When KCl is added, blue water molecules disappear, and only red water molecules remain, resembling the canonical air–water interface. The increase in the number of orange connections between BIL water molecules from the neat to the electrolytic interface illustrates how ions increase in-plane H bonding within the BIL. (B) Evolution with time of the number of water molecules (N_{\max}) that are interconnected by intra-BIL HBs into one single 2D-HB-network, normalized by the average number of water in the BIL ($\langle N_{\text{BIL}} \rangle$). Red, reference air–water interface; blue, silica–water + KCl interface. A similar plot is not reported for the neat silica–water interface, as the 2D-HB-network does not exist at that interface. (C) Innersphere adsorption of the KCl ion-pair at the SiO₂–water interface. The ions use silanols (red balls for the oxygens) and water in the BIL (blue balls for the oxygens) in order to achieve an innersphere adsorption.

the canonical hydrophobic air–water interface,⁵⁴ where 1.7 intra-BIL HBs are also found on average.^{55,60} The time-evolution for the formation of the 2D-HB-network at the silica–water interface (Figure 3C) reveals that the number of intra-BIL HB/molecule increases in a few picoseconds, from 1.2 (neat interface, start of the dynamics) to 1.7, by adding one KCl ion-pair in the BIL.

The electrolyte-induced increase in water interconnectivity is further illustrated in Figure 4A where top views of the BIL water molecules (20 on average in these simulation boxes) of the neat SiO₂–water (left), the SiO₂–water+KCl (middle), and the air–water interface (right; taken from refs 54 and 55; be aware of the larger simulation box) are compared. One can immediately observe the 60%/40% ratio between the two water populations discussed above at the neat solution interface (Figure 4A, left), with the isolated blue-waters above the hydrophobic patches (which are too small for water to form a 2D-HB-network) on one hand and the locally interconnected, tetrahedral red-waters above the hydrophilic patches on the other hand. Once the electrolytes are present in

the BIL (pink/green balls in Figure 4A, middle), one immediately observes the disappearance of the blue-undercoordinated water molecules, and the increased HB interconnectivity in between the red-water molecules, now 3-fold coordinated and extended over the whole silica surface. This is similar to the HB interconnectivity at the air–water interface^{54,55} (Figure 4A, right).

To understand the time-dependent behavior of the HB network of the KCl–silica–water interface with respect to the air–water, we further compare in Figure 4B the time-evolution of the 2D-HB-network size (N_{\max}), normalized by the average number of BIL water molecules ($\langle N_{\text{BIL}} \rangle$) ($\langle N_{\text{BIL}} \rangle = 45$ and 20, respectively, at the air–water and silica–water interfaces). One can see that the two interfaces behave similarly over time, with the normalized 2D-HB-network size steadily varying between 0.8 and 1.0 during the whole simulation.

We can hence conclude that innersphere adsorbed ions alter the water organization in the BIL by shifting the balance from dominant water–surface interactions (“out-of-plane ordering”) to in-plane water–water interactions (“in-plane ordering”). Our molecular picture is consistent with previous theoretical studies^{61–63} showing that adsorbed ions can reorder the interfacial H-bonding network at the quartz (101)–water interface by promoting the formation of intrasurface H-bonds and disrupting the surface water H-bonds. This drives an inhomogeneous interfacial water coordination landscape toward a homogeneous, highly interconnected in-plane 2D hydrogen bonding network, reminiscent of the canonical, hydrophobic air–water interface.

Connecting TR-vSFG and AIMD. We now make use of the structural knowledge obtained from the simulations to provide a rationalization for the T_1 lifetime acceleration upon ion addition at pH 2. The MD simulations demonstrated that there is no DL contribution to the vSFG at the fully hydroxylated (pH 2) silica–water interface and hence confirmed that the acceleration of interfacial relaxation dynamics can only be due to the ion-induced changes in the BIL structure, which in turn alter the intermolecular coupling and affect the BIL dynamics. In more details, we have seen that ions change both water–water interactions and SiOH–water interactions. The question remains as to which is responsible for the experimentally measured changes in T_1 . The SiOH vibrations are expected to exhibit slower relaxation dynamics than OH vibrations of water as the former do not have access to Fermi resonance coupling (which is known to be a major OH vibrational relaxation pathway^{51,64–68}) into its SiOH bend overtone due to the large energy mismatch. The SiOH bend mode is at ~ 800 cm^{-1} , and thus, its overtone is at ~ 1600 cm^{-1} , which is far away from the SiOH stretch vibrational modes (>3000 cm^{-1}).⁵⁶ This is consistent with time-resolved measurements done in the 1980s by Cavanagh et al.⁶⁹ which determined the vibrational lifetime for hydroxyls at the silica–vacuum interface as ~ 200 ps, which decreased to ~ 56 ps in the presence of significant amounts of physisorbed water ($5 \text{ H}_2\text{O}/100 \text{ \AA}^2$). In our study, the silica hydroxyls are H-bonded to adjacent water and thus are expected to have a shorter vibrational lifetime than ~ 200 ps, but it is highly unlikely to be anywhere close to the 100s of femtosecond time-scales we measure. Moreover, SiOH–water couplings are weakened by increasing ion concentration due to ion breaking of water–surface HBs (as discussed before). This would reasonably provoke a slowdown in the SiOH relaxation due to reduced connections to the aqueous environment. In light of all of this,

SiOH group dynamics would explain an increase in T_1 , not a decrease (as observed experimentally). Based on this, we can argue that the SiOH–water coupling contribution to the overall relaxation within the BIL is much less important than the one from water–water couplings. This is consistent with the fact that water molecules in the BIL are much more abundant than surface silanols (from MD simulations, we calculate an average of 12.4 BIL waters/ nm^2 vs 4.5 SiOH/ nm^2), as well as with water providing the dominant contribution to the vSFG intensity of silica–water interfaces in the OH-stretching region. From integration of the theoretical vSFG spectra,^{29,47} we find that water contributes 76% of the imaginary $\chi^{(2)}$ vSFG spectra in the 3000–3800 cm^{-1} range, while surface SiOH groups only contribute 24% at frequencies <3300 cm^{-1} . This 24% value is further reduced to $\sim 6\%$ when considering that we are measuring the $|\chi^{(2)}|^2$ signal in this study.

What remain to be evaluated are the ion-induced water–water couplings within the BIL as the reason for the acceleration of T_1 at pH 2 (and 6) when ions are introduced. As mentioned above, Fermi resonance coupling is known to be a major OH vibrational relaxation pathway.^{51,64–68} Since the H_2O bend mode is at ~ 1650 cm^{-1} (and so its overtone is at ~ 3300 cm^{-1} , without accounting for anharmonicity), there is Fermi resonance coupling between the H_2O stretch vibrations and the H_2O bend. Therefore, an ion-induced increase in water–water interactions is expected to lead to efficient coupling thereby accelerating the vibrational energy transfer and causing a decrease in T_1 . Additional evidence comes from comparing the BIL water structure and T_1 lifetimes at the silica–water and the air–water interfaces. As discussed previously, the BIL structure at the air–water interface is dominated by water–water couplings resulting in a 2D-HB-network, and the T_1 for this hydrogen bonded water has been experimentally measured to be 200–300 fs.^{70–73} Similarly, ion-induced water–water coupling resulting in a 2D-HB-network is detected for the silica–water interface, and consequently, T_1 of 250 fs is also measured. This correlation between the BIL structure and the T_1 lifetime at two different interfaces supports our claim that ion-induced water–water coupling is responsible for the reduction of T_1 .

We further suggest that the acceleration of interfacial relaxation processes with increasing NaCl concentration is justified not only by the ion-induced increased HB-connectivity within the BIL (increased water–water couplings) but also by the net reduction in the number of “strongly undercoordinated” water molecules at the interface (blue water in Figure 4), which are expected to have the slowest relaxation due to the reduced connectivity with the environment.

In light of these findings, the slow T_1 lifetime ($T_1 = 577 \pm 140$ fs) measured for the neat interface at pH 2 conditions can be ascribed to the substantial density of undercoordinated water molecules (40%) and weak H-bond interconnectivity within the out-of-plane ordered BIL. The ion-induced in-plane ordering provokes the acceleration in the vibrational relaxation processes within the BIL, from $T_1 \sim 600$ fs, typical of the water out-of-plane ordering, to $T_1 \sim 250$ fs, typical of the water in-plane ordering, that is reminiscent of the fast vibrational relaxation measured for the air–water interface. The same microscopic mechanism revealed for pH 2 also rationalizes the acceleration of T_1 at pH 6 in the presence of high salt concentration. Such an acceleration at pH 6 has been observed previously²² and was hypothesized to be due to ion-induced

interfacial ordering, but in this study, we are able to provide, for the first time, a molecular mechanism that explains the T_1 acceleration at the silica–electrolyte interface. Even though we are mainly probing the BIL water at pH 2 and pH 6 (with salt), it is important to note that the absolute values of T_1 are not strictly identical (Figure 2B), presumably reflecting the structural variations of surface silanol groups at the two pH conditions, including the difference in the ionic species enrichment at the neutral vs charged silica surface (see the scheme in Figure 2).⁷⁵ Nevertheless, the ratio in the T_1 values at the two ionic concentrations is identical: water systematically relaxes 1.7 times faster at the higher 0.5 M ionic concentration due to the highly interconnected 2D-HB-network formed in the BIL.

Finally, the transition from out-of-plane to in-plane ordering of BIL water due to breaking of water–surface HBs (vSFG active since oriented along the normal to the surface) and consequent formation of intra-BIL water–water H-bonds (non-vSFG active due to the orientation parallel to the surface) also explains the microscopic origin of the previously discussed decrease (albeit small) of the SS-vSFG (ppp) signal when ions adsorb at the neutral silica–water interface.³⁵

CONCLUSIONS

In conclusion, the interplay between experimental vibrational dynamics measurements and the interfacial structural characterization by theory provides a compelling combination to reveal the ion adsorption process at silica–water interfaces and its effect on interfacial structure and dynamics, as a function of pH/electrolyte conditions. At highly and moderately charged silica–water interfaces (pH > 6), cations are preferentially adsorbed at the surface, and their major impact on the interfacial arrangement is screening the surface charge, as expected from GC theory. However, more subtle molecular changes in the BIL are hidden below the dominant DL contribution at these high pH conditions. As revealed by both experiments and simulations performed in this work, such changes manifest at low surface charges (pH < 6) and high ionic concentrations, and they cannot be rationalized by pure electrostatic models as they are driven by local chemistry associated with the ion adsorption processes.

We here show, for the first time, that the acceleration of interfacial vibrational energy relaxation is due to the kosmotropic effect of ions that drive in-plane ordering of water within the BIL, the topmost interfacial layer. This deeper understanding of such a phenomenon, which is beyond the existing GC/SGC theories, represents a key ingredient in the development of more accurate models for describing electrolytic interfaces. Ions such as KCl and NaCl are hence shown to be able to form innersphere complexes at the silica surface, even at low pH (i.e., around PZC) conditions. This requires breaking of previously existing water–surface HBs, thereby forming local “hydrophobic” areas on the silica surface, which adds to the already present hydrophobic patches (silanol poor areas) in the BIL. In such ion-induced hydrophobic domains, water rearranges by forming the extended 2D-HB-network, similar to the canonical air–water interface. TR-vSFG experiments, directly probing interfacial vibrational dynamics, are shown to be a powerful tool to reveal such BIL structural transitions, which is modulated by the delicate balance between water–surface and water–water interactions and is marked by the ion-induced acceleration of interfacial vibrational relaxation.

The methodology employed here for aqueous silica interfaces can be broadly applied to reveal the kosmotropic/chaotropic nature of ions at other aqueous interfaces: TR-vSFG experiments provide a direct measure of BIL water ordering/disordering, while DFT-MD simulations unveil the underlying microscopic mechanisms.

ASSOCIATED CONTENT

Supporting Information

The Supporting Information is available free of charge at <https://pubs.acs.org/doi/10.1021/jacs.9b13273>.

Experimental and theoretical methods, additional information on the experimental vSFG setup and sample preparation, the model used to describe vibrational dynamics of O–H in water, calculations of the surface electric potential at the silica–water interface, AIMD/DFT-based molecular dynamics simulations and their interpretation in terms of BIL (binding interfacial layer) and DL (diffuse layer), and the model used to separate BIL/DL contributions to TR-vSFG (PDF)

AUTHOR INFORMATION

Corresponding Authors

Marie-Pierre Gaigeot – LAMBE UMR8587, Université d'Evry val d'Essonne, CNRS, CEA, Université Paris-Saclay, 91025 Evry, France; orcid.org/0000-0002-3409-5824; Email: mgaigeot@univ-evry.fr

Eric Borguet – Department of Chemistry, Temple University, Philadelphia, Pennsylvania 19122, United States; orcid.org/0000-0003-0593-952X; Email: eborguet@temple.edu

Authors

Aashish Tuladhar – Physical Sciences Division, Physical & Computational Sciences Directorate, Pacific Northwest National Laboratory, Richland, Washington 99352, United States; Department of Chemistry, Temple University, Philadelphia, Pennsylvania 19122, United States; orcid.org/0000-0003-2449-4984

Shalaka Dewan – Department of Chemistry, Temple University, Philadelphia, Pennsylvania 19122, United States

Simone Pezzotti – LAMBE UMR8587, Université d'Evry val d'Essonne, CNRS, CEA, Université Paris-Saclay, 91025 Evry, France

Flavio Siro Brigiano – LAMBE UMR8587, Université d'Evry val d'Essonne, CNRS, CEA, Université Paris-Saclay, 91025 Evry, France

Fabrizio Creazzo – LAMBE UMR8587, Université d'Evry val d'Essonne, CNRS, CEA, Université Paris-Saclay, 91025 Evry, France

Complete contact information is available at: <https://pubs.acs.org/doi/10.1021/jacs.9b13273>

Author Contributions

^{||}A.T., S.D., and S.P. contributed equally to this work.

Notes

The authors declare no competing financial interest.

ACKNOWLEDGMENTS

The authors acknowledge the National Science Foundation for supporting this work (NSF Grants CHE 1337880 and MRI 1828421) and thank Dr. Ali Eftekhari-Bafrooei for helpful discussions and Dr. Mark DelloStritto for helping in making

the contour plots. A.T. acknowledges the support provided by the US Department of Energy (DOE), Office of Science, Office of Basic Energy Sciences, Materials Sciences and Engineering Division and Chemical Sciences, Geosciences, and Biosciences Division at The Pacific Northwest National Laboratory, operated by Battelle for the US Department of Energy (DOE) under Contract DE-AC05-76RL01830. HPC resources from GENCI-France Grant 072484 (CINES/IDRIS/TGCC) are acknowledged. S.P., F.S.B., F.C., and M.-P.G. acknowledge that this work was done under funding by ANR DYNWIN Grant 14-CE35-0011-01 and LABEX CHARMA₃T 11- LABEX-0039/ANR-11-IDEX-0003-02 "Excellence Laboratory" program of the University Paris-Saclay. The authors thank Dr. Daria Ruth Galimberti for discussions and advice.

REFERENCES

- (1) Dessler, A. E.; Sherwood, S. C. A Matter of Humidity. *Science* **2009**, *323*, 1020–1021.
- (2) Jung, M.; Reichstein, M.; Schwalm, C. R.; Huntingford, C.; Sitch, S.; Ahlström, A.; Arneth, A.; Camps-Valls, G.; Ciais, P.; Friedlingstein, P.; Gans, F.; Ichii, K.; Jain, A. K.; Kato, E.; Papale, D.; Poulter, B.; Raduly, B.; Rödenbeck, C.; Tramontana, G.; Viovy, N.; Wang, Y.-P.; Weber, U.; Zaehle, S.; Zeng, N. Compensatory Water Effects Link Yearly Global Land CO₂ Sink Changes to Temperature. *Nature* **2017**, *541*, 516–520.
- (3) Ball, P. Water is an Active Matrix of Life for Cell and Molecular Biology. *Proc. Natl. Acad. Sci. U. S. A.* **2017**, *114*, 13327–13335.
- (4) Maddox, J. Putting Molecular Biology into Water. *Nature* **1993**, *364*, 669.
- (5) Chaplin, M. Do We Underestimate the Importance of Water in Cell Biology? *Nat. Rev. Mol. Cell Biol.* **2006**, *7*, 861–866.
- (6) Chen, S.; Itoh, Y.; Masuda, T.; Shimizu, S.; Zhao, J.; Ma, J.; Nakamura, S.; Okuro, K.; Noguchi, H.; Uosaki, K.; Aida, T. Subnanoscale Hydrophobic Modulation of Salt Bridges in Aqueous Media. *Science* **2015**, *348*, 555–559.
- (7) Ojha, L.; Wilhelm, M. B.; Murchie, S. L.; McEwen, A. S.; Wray, J. J.; Hanley, J.; Massé, M.; Chojnacki, M. Spectral Evidence for Hydrated Salts in Recurring Slope Lineae on Mars. *Nat. Geosci.* **2015**, *8*, 829–832.
- (8) McEwen, A. S.; Ojha, L.; Dundas, C. M.; Mattson, S. S.; Byrne, S.; Wray, J. J.; Cull, S. C.; Murchie, S. L.; Thomas, N.; Gulick, V. C. Seasonal Flows on Warm Martian Slopes. *Science* **2011**, *333*, 740–743.
- (9) Sposito, G.; Skipper, N. T.; Sutton, R.; Park, S.-h.; Soper, A. K.; Greathouse, J. A. Surface Geochemistry of the Clay Minerals. *Proc. Natl. Acad. Sci. U. S. A.* **1999**, *96*, 3358–3364.
- (10) Pekel, J.-F.; Cottam, A.; Gorelick, N.; Belward, A. S. High-Resolution Mapping of Global Surface Water and its Long-Term Changes. *Nature* **2016**, *540*, 418–422.
- (11) Tunuguntla, R. H.; Henley, R. Y.; Yao, Y.-C.; Pham, T. A.; Wanunu, M.; Noy, A. Enhanced Water Permeability and Tunable Ion Selectivity in Subnanometer Carbon Nanotube Porins. *Science* **2017**, *357*, 792–796.
- (12) Franzese, G.; Bianco, V. Water at Biological and Inorganic Interfaces. *Food Biophys.* **2013**, *8*, 153–169.
- (13) Shelton, D. P. Water-Water Correlations in Electrolyte Solutions Probed by Hyper-Rayleigh Scattering. *J. Chem. Phys.* **2017**, *147*, 214505.
- (14) Chen, Y.; Okur, H. I.; Dupertuis, N.; Dedic, J.; Wilkins, D. M.; Ceriotti, M.; Roke, S. Comment on "Water-Water Correlations in Electrolyte Solutions Probed by Hyper-Rayleigh Scattering" [*J. Chem. Phys.* **147**, 214505 (2017)]. *J. Chem. Phys.* **2018**, *149*, 167101.
- (15) Shelton, D. P. Response to "Comment on 'Water-Water Correlations in Electrolyte Solutions Probed by Hyper-Rayleigh Scattering'" [*J. Chem. Phys.* **149**, 167101 (2018)]. *J. Chem. Phys.* **2018**, *149*, 167102.
- (16) Chan, Y. C.; Wong, K. Y. Study of the Pair Correlations Between P-Nitroaniline Molecules in Solution by Depolarized Hyper-Rayleigh Scattering. *J. Chem. Phys.* **2012**, *136*, 174514.
- (17) O'Brien, J. T.; Williams, E. R. Effects of Ions on Hydrogen-Bonding Water Networks in Large Aqueous Nanodrops. *J. Am. Chem. Soc.* **2012**, *134*, 10228–10236.
- (18) Smith, J. D.; Saykally, R. J.; Geissler, P. L. The Effects of Dissolved Halide Anions on Hydrogen Bonding in Liquid Water. *J. Am. Chem. Soc.* **2007**, *129*, 13847–13856.
- (19) Lin, Y. S.; Auer, B. M.; Skinner, J. L. Water Structure, Dynamics, and Vibrational Spectroscopy in Sodium Bromide Solutions. *J. Chem. Phys.* **2009**, *131*, 144511.
- (20) Omta, A. W.; Kropman, M. F.; Woutersen, S.; Bakker, H. J. Negligible Effect of Ions on the Hydrogen-Bond Structure in Liquid Water. *Science* **2003**, *301*, 347–349.
- (21) Eftekhari-Bafrooei, A.; Borguet, E. Effect of Surface Charge on the Vibrational Dynamics of Interfacial Water. *J. Am. Chem. Soc.* **2009**, *131*, 12034–12035.
- (22) Eftekhari-Bafrooei, A.; Borguet, E. Effect of Electric Fields on the Ultrafast Vibrational Relaxation of Water at a Charged Solid-Liquid Interface as Probed by Vibrational Sum Frequency Generation. *J. Phys. Chem. Lett.* **2011**, *2*, 1353–1358.
- (23) Ohno, P. E.; Chang, H.; Spencer, A. P.; Liu, Y.; Boamah, M. D.; Wang, H.-f.; Geiger, F. M. Beyond the Gouy-Chapman Model with Heterodyne-Detected Second Harmonic Generation. *J. Phys. Chem. Lett.* **2019**, *10*, 2328–2334.
- (24) Darlington, A. M.; Jarisz, T. A.; Dewalt-Kerian, E. L.; Roy, S.; Kim, S.; Azam, M. S.; Hore, D. K.; Gibbs, J. M. Separating the pH-Dependent Behavior of Water in the Stern and Diffuse Layers with Varying Salt Concentration. *J. Phys. Chem. C* **2017**, *121*, 20229–20241.
- (25) DeWalt-Kerian, E. L.; Kim, S.; Azam, M. S.; Zeng, H. B.; Liu, Q. X.; Gibbs, J. M. pH-Dependent Inversion of Hofmeister Trends in the Water Structure of the Electrical Double Layer. *J. Phys. Chem. Lett.* **2017**, *8*, 2855–2861.
- (26) Macias-Romero, C.; Nahalka, I.; Okur, H. I.; Roke, S. Optical Imaging of Surface Chemistry and Dynamics in Confinement. *Science* **2017**, *357*, 784–788.
- (27) Chapman, D. L. A Contribution to the Theory of Electrocapillarity. *Philos. Mag.* **1913**, *25*, 475–481.
- (28) Grahame, D. C. The Electrical Double Layer and the Theory of Electrocapillarity. *Chem. Rev.* **1947**, *41*, 441–501.
- (29) Cyran, J. D.; Donovan, M. A.; Vollmer, D.; Siro Brigiano, F.; Pezzotti, S.; Galimberti, D. R.; Gaigeot, M.-P.; Bonn, M.; Backus, E. H. G. Molecular Hydrophobicity at a Macroscopically Hydrophilic Surface. *Proc. Natl. Acad. Sci. U. S. A.* **2019**, *116*, 1520–1525.
- (30) Covert, P. A.; Jena, K. C.; Hore, D. K. Throwing Salt into the Mix: Altering Interfacial Water Structure by Electrolyte Addition. *J. Phys. Chem. Lett.* **2014**, *5*, 143–148.
- (31) Jena, K. C.; Covert, P. A.; Hore, D. K. The Effect of Salt on the Water Structure at a Charged Solid Surface: Differentiating Second- and Third-order Nonlinear Contributions. *J. Phys. Chem. Lett.* **2011**, *2*, 1056–1061.
- (32) Hore, D. K.; Tyrode, E. Probing Charged Aqueous Interfaces Near Critical Angles: Effect of Varying Coherence Length. *J. Phys. Chem. C* **2019**, *123*, 16911–16920.
- (33) Dalstein, L.; Potapova, E.; Tyrode, E. The Elusive Silica/Water Interface: Isolated Silanols Under Water as Revealed by Vibrational Sum Frequency Spectroscopy. *Phys. Chem. Chem. Phys.* **2017**, *19*, 10343–10349.
- (34) Du, Q.; Freysz, E.; Shen, Y. R. Vibrational Spectra of Water Molecules at Quartz/Water Interfaces. *Phys. Rev. Lett.* **1994**, *72*, 238–241.
- (35) Dewan, S.; Yeganeh, M. S.; Borguet, E. Experimental Correlation Between Interfacial Water Structure and Mineral Reactivity. *J. Phys. Chem. Lett.* **2013**, *4*, 1977–1982.
- (36) Yang, Z.; Li, Q.; Chou, K. C. Structures of Water Molecules at the Interfaces of Aqueous Salt Solutions and Silica: Cation Effects. *J. Phys. Chem. C* **2009**, *113*, 8201–8205.

- (37) Myalitsin, A.; Urashima, S.-h.; Nihonyanagi, S.; Yamaguchi, S.; Tahara, T. Water Structure at the Buried Silica/Aqueous Interface Studied by Heterodyne-Detected Vibrational Sum-Frequency Generation. *J. Phys. Chem. C* **2016**, *120*, 9357–9363.
- (38) Ostroverkhov, V.; Waychunas, G. A.; Shen, Y. R. Vibrational Spectra of Water at Water/ α -Quartz (0001) Interface. *Chem. Phys. Lett.* **2004**, *386*, 144–148.
- (39) Lis, D.; Backus, E. H. G.; Hunger, J.; Parekh, S. H.; Bonn, M. Liquid Flow Along a Solid Surface Reversibly Alters Interfacial Chemistry. *Science* **2014**, *344*, 1138–1142.
- (40) Urashima, S.-h.; Myalitsin, A.; Nihonyanagi, S.; Tahara, T. The Topmost Water Structure at a Charged Silica/Aqueous Interface Revealed by Heterodyne-Detected Vibrational Sum Frequency Generation Spectroscopy. *J. Phys. Chem. Lett.* **2018**, *9*, 4109–4114.
- (41) McGuire, J. A.; Shen, Y. R. Ultrafast Vibrational Dynamics at Water Interfaces. *Science* **2006**, *313*, 1945–1948.
- (42) Eftekhari-Bafrooei, A.; Borguet, E. Effect of Hydrogen-Bond Strength on the Vibrational Relaxation of Interfacial Water. *J. Am. Chem. Soc.* **2010**, *132*, 3756–3761.
- (43) Wen, Y.-C.; Zha, S.; Liu, X.; Yang, S.; Guo, P.; Shi, G.; Fang, H.; Shen, Y. R.; Tian, C. Unveiling Microscopic Structures of Charged Water Interfaces by Surface-Specific Vibrational Spectroscopy. *Phys. Rev. Lett.* **2016**, *116*, 016101.
- (44) Pezzotti, S.; Galimberti, D. R.; Shen, Y. R.; Gaigeot, M.-P. Structural Definition of the BIL and DL: a New Universal Methodology to Rationalize Non-Linear $\chi^{(2)}(\omega)$ SFG Signals at Charged Interfaces, Including $\chi^{(3)}(\omega)$ Contributions. *Phys. Chem. Chem. Phys.* **2018**, *20*, 5190–5199.
- (45) Dove, P. M. The Dissolution Kinetics of Quartz in Sodium Chloride Solutions at 25 Degrees to 300 Degrees C. *Am. J. Sci.* **1994**, *294*, 665–712.
- (46) Pezzotti, S.; Galimberti, D.; Shen, Y.; Gaigeot, M.-P. What the Diffuse Layer (DL) Reveals in Non-Linear SFG Spectroscopy. *Minerals* **2018**, *8*, 305.
- (47) Pezzotti, S.; Galimberti, D. R.; Gaigeot, M.-P. Deconvolution of BIL-SFG and DL-SFG spectroscopic signals reveals order/disorder of water at the elusive aqueous silica interface. *Phys. Chem. Chem. Phys.* **2019**, *21*, 22188–22202.
- (48) Ohno, P. E.; Saslow, S. A.; Wang, H.-f.; Geiger, F. M.; Eienthal, K. B. Phase-Referenced Nonlinear Spectroscopy of the α -Quartz/Water Interface. *Nat. Commun.* **2016**, *7*, 13587.
- (49) Gonella, G.; Lütgebaucks, C.; de Beer, A. G. F.; Roke, S. Second Harmonic and Sum-Frequency Generation from Aqueous Interfaces Is Modulated by Interference. *J. Phys. Chem. C* **2016**, *120*, 9165–9173.
- (50) Fecko, C. J.; Eaves, J. D.; Loparo, J. J.; Tokmakoff, A.; Geissler, P. L. Ultrafast Hydrogen-Bond Dynamics in the Infrared Spectroscopy of Water. *Science* **2003**, *301*, 1698–1702.
- (51) Lock, A. J.; Bakker, H. J. Temperature Dependence of Vibrational Relaxation in Liquid H₂O. *J. Chem. Phys.* **2002**, *117*, 1708–1713.
- (52) Cowan, M. L.; Bruner, B. D.; Huse, N.; Dwyer, J. R.; Chugh, B.; Nibbering, E. T. J.; Elsaesser, T.; Miller, R. J. D. Ultrafast Memory Loss and Energy Redistribution in the Hydrogen Bond Network of Liquid H₂O. *Nature* **2005**, *434*, 199–202.
- (53) Campen, R. K.; Pymmer, A. K.; Nihonyanagi, S.; Borguet, E. Linking Surface Potential and Deprotonation in Nanoporous Silica: Second Harmonic Generation and Acid/Base Titration. *J. Phys. Chem. C* **2010**, *114*, 18465–18473.
- (54) Pezzotti, S.; Galimberti, D. R.; Gaigeot, M.-P. 2D H-Bond Network as the Topmost Skin to the Air–Water Interface. *J. Phys. Chem. Lett.* **2017**, *8*, 3133–3141.
- (55) Pezzotti, S.; Serva, A.; Gaigeot, M.-P. 2D-HB-Network at the Air–Water Interface: A Structural and Dynamical Characterization by Means of Ab Initio and Classical Molecular Dynamics Simulations. *J. Chem. Phys.* **2018**, *148*, 174701.
- (56) Isaienko, O.; Borguet, E. Hydrophobicity of Hydroxylated Amorphous Fused Silica Surfaces. *Langmuir* **2013**, *29*, 7885–7895.
- (57) Pfeiffer-Laplaud, M.; Gaigeot, M.-P. Electrolytes at the Hydroxylated (0001) α -Quartz/Water Interface: Location and Structural Effects on Interfacial Silanols by DFT-Based MD. *J. Phys. Chem. C* **2016**, *120*, 14034–14047.
- (58) Pfeiffer-Laplaud, M.; Gaigeot, M.-P. Adsorption of Singly Charged Ions at the Hydroxylated (0001) α -Quartz/Water Interface. *J. Phys. Chem. C* **2016**, *120*, 4866–4880.
- (59) Wang, R.; DelloStritto, M.; Remsing, R. C.; Carnevale, V.; Klein, M. L.; Borguet, E. Sodium Halide Adsorption and Water Structure at the α -Alumina(0001)/Water Interface. *J. Phys. Chem. C* **2019**, *123*, 15618–15628.
- (60) Serva, A.; Pezzotti, S.; Bougueroua, S.; Galimberti, D. R.; Gaigeot, M.-P. Combining Ab-Initio and Classical Molecular Dynamics Simulations to Unravel the Structure of the 2D-HB-Network at the Air–Water Interface. *J. Mol. Struct.* **2018**, *1165*, 71–78.
- (61) Kubicki, J. D.; Sofo, J. O.; Skelton, A. A.; Bandura, A. V. A New Hypothesis for the Dissolution Mechanism of Silicates. *J. Phys. Chem. C* **2012**, *116*, 17479–17491.
- (62) DelloStritto, M. J.; Kubicki, J. D.; Sofo, J. O. Effect of Ions on H-Bond Structure and Dynamics at the Quartz(101)–Water Interface. *Langmuir* **2016**, *32*, 11353–11365.
- (63) DelloStritto, M. J.; Kubicki, J.; Sofo, J. O. Density Functional Theory Simulation of Hydrogen-Bonding Structure and Vibrational Densities of States at the Quartz (1 0 1)-Water Interface and its Relation to Dissolution as a Function of Solution pH and Ionic Strength. *J. Phys.: Condens. Matter* **2014**, *26*, 244101.
- (64) Lindner, J.; Vöhringer, P.; Pshenichnikov, M. S.; Cringus, D.; Wiersma, D. A.; Mostovoy, M. Vibrational Relaxation of Pure Liquid Water. *Chem. Phys. Lett.* **2006**, *421*, 329–333.
- (65) Ashihara, S.; Huse, N.; Espagne, A.; Nibbering, E. T. J.; Elsaesser, T. Ultrafast Structural Dynamics of Water Induced by Dissipation of Vibrational Energy. *J. Phys. Chem. A* **2007**, *111*, 743–746.
- (66) Bakker, H. J.; Skinner, J. L. Vibrational Spectroscopy as a Probe of Structure and Dynamics in Liquid Water. *Chem. Rev.* **2010**, *110*, 1498–1517.
- (67) Lawrence, C. P.; Skinner, J. L. Vibrational Spectroscopy of HOD in Liquid D₂O. VI. Intramolecular and Intermolecular Vibrational Energy Flow. *J. Chem. Phys.* **2003**, *119*, 1623–1633.
- (68) Rey, R.; Hynes, J. T. Vibrational Energy Relaxation of HOD in Liquid D₂O. *J. Chem. Phys.* **1996**, *104*, 2356–2368.
- (69) Heilweil, E. J.; Casassa, M. P.; Cavanagh, R. R.; Stephenson, J. C. Vibrational Deactivation of Surface OH Chemisorbed on SiO₂: Solvent Effects. *J. Chem. Phys.* **1985**, *82*, 5216–5231.
- (70) Inoue, K.-i.; Ishiyama, T.; Nihonyanagi, S.; Yamaguchi, S.; Morita, A.; Tahara, T. Efficient Spectral Diffusion at the Air/Water Interface Revealed by Femtosecond Time-Resolved Heterodyne-Detected Vibrational Sum Frequency Generation Spectroscopy. *J. Phys. Chem. Lett.* **2016**, *7*, 1811–1815.
- (71) Hsieh, C.-S.; Okuno, M.; Hunger, J.; Backus, E. H. G.; Nagata, Y.; Bonn, M. Aqueous Heterogeneity at the Air/Water Interface Revealed by 2D-HD-SFG Spectroscopy. *Angew. Chem., Int. Ed.* **2014**, *53*, 8146–8149.
- (72) Zhang, Z.; Piatkowski, L.; Bakker, H. J.; Bonn, M. Ultrafast Vibrational Energy Transfer at the Water/Air Interface Revealed by Two-Dimensional Surface Vibrational Spectroscopy. *Nat. Chem.* **2011**, *3*, 888–893.
- (73) Van Der Post, S. T.; Hsieh, C.-S.; Okuno, M.; Nagata, Y.; Bakker, H. J.; Bonn, M.; Hunger, J. Strong Frequency Dependence of Vibrational Relaxation in Bulk and Surface Water Reveals Sub-Picosecond Structural Heterogeneity. *Nat. Commun.* **2015**, *6*, 8384.
- (74) Wang, H.; Xu, Q.; Liu, Z.; Tang, Y.; Wei, G.; Shen, Y. R.; Liu, W.-T. Gate-Controlled Sum-Frequency Vibrational Spectroscopy for Probing Charged Oxide/Water Interfaces. *J. Phys. Chem. Lett.* **2019**, *10* (19), 5943–5948.
- (75) Dewan, S.; Carnevale, V.; Bankura, A.; Eftekhari-Bafrooei, A.; Fiorin, G.; Klein, M. L.; Borguet, E. The Structure of Water at Charged Interfaces: A Molecular Dynamics Study. *Langmuir* **2014**, *30* (27), 8056–8065.